Proceedings of the Canadian Society for Mechanical Engineering International Congress 2021
CSME Congress 2021
June 27-30, 2021, Charlottetown, PE, Canada

Attitude dynamics model of a CubeSat with reaction wheels for an extended Kalman filter

Robert Bauer
Department of Mechanical Engineering
Dalhousie University
Halifax, Canada
robert.bauer@dal.ca

***Abstract*—This paper presents a derivation of the attitude dynamics equations of motion of a CubeSat with reaction wheels. The rigid-body equations of motion can be extended to any number of arbitrarily-oriented and arbitrarily-located reaction wheels. The equations of motion are implemented and validated using numerical simulations. It is then shown how the resulting equations of motion can be propagated within a quaternion-based extended Kalman filter. This filter combines attitude quaternion and angular velocity measurements with the derived attitude dynamics model. For the simulation conditions used in this research, the filter provides an improved estimate of the CubeSat's attitude quaternion and angular rates.**

***Index Terms*—attitude dynamics, extended Kalman filter, derivation, equations of motion, reaction wheels**

I. Introduction

Accurate attitude determination is becoming increasingly important for CubeSats as their payloads become more advanced [1]. The extended Kalman filter (EKF) is often used in spacecraft attitude estimation [2]. While Kalman filters can be implemented without incorporating the attitude dynamics equations [3], Yang and Zhou [4] suggest that including the spacecraft dynamics in the EKF can yield improved attitude estimates.

This paper derives the spacecraft attitude dynamics equations of motion for a rigid body with n reaction wheels and is based on the derivation presented by Hughes [5] for a rigid body with a rotating wheel using his "vectrix" notation convention. The resulting dynamics model is validated for an example CubeSat with a non-diagonal inertia matrix and three reaction wheels.

The paper then shows how these equations of motion can be implemented within a quaternion-based EKF. The developed EKF is based on the formulation presented by Yang [2] but instead of using a reduced quaternion model it includes all four attitude quaternion components and incorporates the attitude dynamics model derived in this paper. With this full-quaternion model, the resulting EKF can be applied to a tumbling satellite without any limits placed on the range of satellite orientations.

II. Derivation of equations of motion

This derivation of the equations of motion of a CubeSat with reaction wheels is based on the "gyrostat" derivation presented by Hughes [5] and uses similar notation. Referring to Fig. 1, let $\mathcal{R}$ correspond to a rigid body without wheels, and $\mathcal{W}_i$ $(i = 1, 2...n)$ be axially-symmetric rotors or wheels which have been mounted to $\mathcal{R}$. The goal of this derivation is to formulate the equations of motion as nonlinear state-space equations for subsequent use in an EKF.

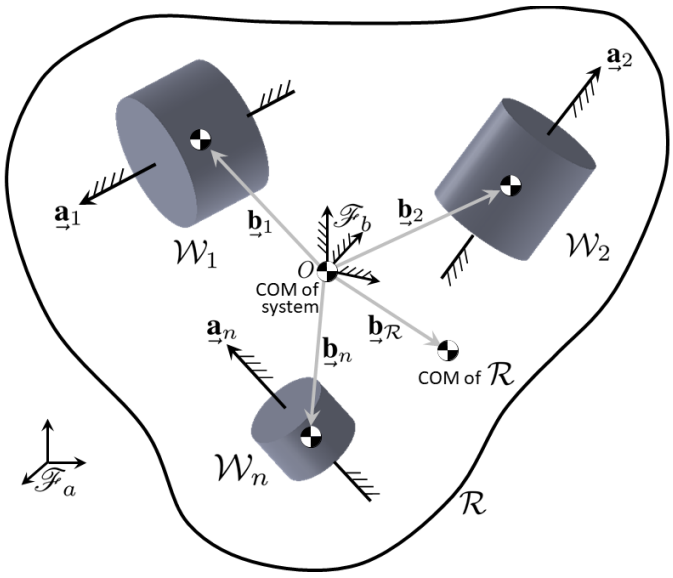

Fig. 1. Rigid body $\mathcal{R}$ with arbitrarily positioned and oriented wheels $\mathcal{W}_i$, $i = 1..n$ fixed in $\mathcal{R}$

Referring to Fig. 1, $\mathscr{F}_a$ is the Earth-centered inertial (ECI) frame of reference and $\mathscr{F}_b$ is a body-fixed (BF) frame fixed in $\mathcal{R}$ at the center of mass (COM) O of the entire system $\mathcal{R} + \mathcal{W}_1 + \mathcal{W}_2 + ... + \mathcal{W}_n$. Frame $\mathscr{F}_b$ should be conveniently oriented within $\mathcal{R}$ since all vectors will be ultimately expressed in this BF frame. In terms of notation, bold font corresponds to vectors, column matrices, dyadics and matrices, while non-bold font corresponds to scalars. Let $\underset{\rightarrow}{\boldsymbol{I}}_{\mathcal{R}}$ be the second-moment-of-inertia dyadic of $\mathcal{R}$ about the COM of $\mathcal{R}$ (without wheels), and $\underset{\rightarrow}{\mathbf{J}}_b$ be the second-moment-of-inertia dyadic of $\mathcal{R}$ about O. These two dyadics can be related using the parallel-axis theorem

$$\underset{\rightarrow}{\mathbf{J}}_b = \underset{\rightarrow}{\boldsymbol{I}}_{\mathcal{R}} + m_{\mathcal{R}} \left(b_{\mathcal{R}}^2 \underset{\rightarrow}{\mathbf{1}} - \underset{\rightarrow}{\mathbf{b}}_{\mathcal{R}} \underset{\rightarrow}{\mathbf{b}}_{\mathcal{R}} \right) \tag{1}$$

where $m_{\mathcal{R}}$ is the mass of $\mathcal{R}$, $\underset{\rightarrow}{\mathbf{b}}_{\mathcal{R}}$ is the vector with magnitude $b_{\mathcal{R}}$ from O to the COM of $\mathcal{R}$, and $\underset{\rightarrow}{\mathbf{1}}$ is the unit dyadic.

Let $m_{\mathcal{W}i}$ be the mass of $\mathcal{W}_i$, I_{si} be the scalar second moment of inertia of $\mathcal{W}_i$ about its axis of symmetry defined by the arbitrarily-oriented spin axis $\underset{\rightarrow}{\mathbf{a}}_i$ (where $\underset{\rightarrow}{\mathbf{a}}_i$ is a unit vector fixed in $\mathcal{R}$), and I_{ti} be the scalar second moment of inertia of $\mathcal{W}_i$ about any transverse axis to $\underset{\rightarrow}{\mathbf{a}}_i$. Then the second-moment-of-inertia dyadic of $\mathcal{W}_i$ about the COM of $\mathcal{W}_i$ is given by [5]

$$\underset{\rightarrow}{\boldsymbol{I}}_{\mathcal{W}i} = I_{ti}\underset{\rightarrow}{\mathbf{1}} + (I_{si} - I_{ti})\underset{\rightarrow}{\mathbf{a}}_i\underset{\rightarrow}{\mathbf{a}}_i \ , \ i = 1...n \tag{2}$$

Furthermore, the second moment of inertia dyadic of the entire system $\mathcal{R}+\mathcal{W}_i$ about O (again using the parallel-axis theorem) is given by

$$\underset{\rightarrow}{\mathbf{J}} = \underset{\rightarrow}{\mathbf{J}}_b + \sum_{i=1}^{n}\left[\underset{\rightarrow}{\boldsymbol{I}}_{\mathcal{W}i} + m_{\mathcal{W}i}\left(b_i^2\underset{\rightarrow}{\mathbf{1}} - \underset{\rightarrow}{\mathbf{b}}_i\underset{\rightarrow}{\mathbf{b}}_i\right)\right] \tag{3}$$

where $\underset{\rightarrow}{\mathbf{b}}_i$ is the vector with magnitude b_i from O to the COM of $\mathcal{W}_i$.

The system $\mathcal{R}+\mathcal{W}_i$ has a total of $3+n$ degrees of freedom (DOF): three DOF associated with the rotation of $\mathcal{R}$ about O, and n DOF associated with the rotation of wheels $\mathcal{W}_i$, $i = 1...n$ about their respective spin axes $\underset{\rightarrow}{\mathbf{a}}_i$. The resulting $3+n$ equations of motion can be derived from the rate of change of momentum equations [5]

$$\dot{\underset{\rightarrow}{\mathbf{h}}} = \underset{\rightarrow}{\mathbf{g}} \tag{4}$$

$$\dot{h}_{ai} = g_{ai} \ , \ i = 1...n \tag{5}$$

where $\dot{\underset{\rightarrow}{\mathbf{h}}}$ is the time derivative measured in $\mathscr{F}_a$ of the absolute angular momentum of $\mathcal{R}+\mathcal{W}_i$ about O, $\dot{h}_{ai}$ is the component along the rotor spin axis $\underset{\rightarrow}{\mathbf{a}}_i$ of the rate of change of the absolute angular momentum of $\mathcal{W}_i$ about the COM of $\mathcal{W}_i$, $\underset{\rightarrow}{\mathbf{g}}$ is the external torque on $\mathcal{R}$, and g_{ai} is the axial torque from the i^{th} reaction wheel motor on $\mathcal{W}_i$ about spin axis $\underset{\rightarrow}{\mathbf{a}}_i$.

The three equations of motion given by (4) can be written in terms of angular velocities by recognizing that, with O located at the COM of the entire system $\mathcal{R}+\mathcal{W}_i$, the total absolute angular momentum about O is given by [5]

$$\underset{\rightarrow}{\mathbf{h}} = \underset{\rightarrow}{\mathbf{J}}\cdot\underset{\rightarrow}{\boldsymbol{\omega}} + \sum_{i=1}^{n}\underset{\rightarrow}{\mathbf{a}}_i I_{si}\omega_{si} \tag{6}$$

where $\underset{\rightarrow}{\boldsymbol{\omega}}$ is the absolute angular velocity of $\mathcal{R}$ (with respect to $\mathscr{F}_a$), and ω_{si} is the relative angular speed of $\mathcal{W}_i$ with respect to $\mathcal{R}$ about its spin axis $\underset{\rightarrow}{\mathbf{a}}_i$ corresponding to the speed of the i^{th} reaction wheel.

Let $\mathring{\underset{\rightarrow}{\mathbf{h}}}$ be the time derivative of $\underset{\rightarrow}{\mathbf{h}}$ measured in $\mathscr{F}_b$. Then

$$\dot{\underset{\rightarrow}{\mathbf{h}}} = \mathring{\underset{\rightarrow}{\mathbf{h}}} + \underset{\rightarrow}{\boldsymbol{\omega}}\times\underset{\rightarrow}{\mathbf{h}} \tag{7}$$

Substituting (4) into (7) and rearranging for $\mathring{\underset{\rightarrow}{\mathbf{h}}}$ results in

$$\mathring{\underset{\rightarrow}{\mathbf{h}}} = -\underset{\rightarrow}{\boldsymbol{\omega}}\times\underset{\rightarrow}{\mathbf{h}} + \underset{\rightarrow}{\mathbf{g}} \tag{8}$$

Taking the time derivative measured in $\mathscr{F}_b$ of (6) (while recognizing that dyadic $\mathring{\underset{\rightarrow}{\mathbf{J}}} = \underset{\rightarrow}{\mathbf{0}}$, vector $\mathring{\underset{\rightarrow}{\mathbf{a}}}_i = \underset{\rightarrow}{\mathbf{0}}$, scalar $\mathring{I}_{si} \equiv \dot{I}_{si} = 0$, and scalar $\mathring{\omega}_{si} \equiv \dot{\omega}_{si}$) gives

$$\mathring{\underset{\rightarrow}{\mathbf{h}}} = \underset{\rightarrow}{\mathbf{J}}\cdot\mathring{\underset{\rightarrow}{\boldsymbol{\omega}}} + \sum_{i=1}^{n}\underset{\rightarrow}{\mathbf{a}}_i I_{si}\dot{\omega}_{si} \tag{9}$$

Equating (8) and (9) yields

$$\underset{\rightarrow}{\mathbf{J}}\cdot\mathring{\underset{\rightarrow}{\boldsymbol{\omega}}} + \sum_{i=1}^{n}\underset{\rightarrow}{\mathbf{a}}_i I_{si}\dot{\omega}_{si} = -\underset{\rightarrow}{\boldsymbol{\omega}}\times\underset{\rightarrow}{\mathbf{h}} + \underset{\rightarrow}{\mathbf{g}} \tag{10}$$

Recognizing that $\dot{\underset{\rightarrow}{\boldsymbol{\omega}}} = \mathring{\underset{\rightarrow}{\boldsymbol{\omega}}} + \underset{\rightarrow}{\boldsymbol{\omega}}\times\underset{\rightarrow}{\boldsymbol{\omega}} = \mathring{\underset{\rightarrow}{\boldsymbol{\omega}}}$, then (6) can be substituted into (10) and rearranged to give

$$\underset{\rightarrow}{\mathbf{J}}\cdot\dot{\underset{\rightarrow}{\boldsymbol{\omega}}} = -\underset{\rightarrow}{\boldsymbol{\omega}}\times\left(\underset{\rightarrow}{\mathbf{J}}\cdot\underset{\rightarrow}{\boldsymbol{\omega}} + \sum_{i=1}^{n}\underset{\rightarrow}{\mathbf{a}}_i I_{si}\omega_{si}\right) + \underset{\rightarrow}{\mathbf{g}} - \sum_{i=1}^{n}\underset{\rightarrow}{\mathbf{a}}_i I_{si}\dot{\omega}_{si} \tag{11}$$

This equation of motion contains two angular velocity derivative terms $\dot{\underset{\rightarrow}{\boldsymbol{\omega}}}$ and $\dot{\omega}_{si}$. To relate these two terms note that the component along the rotor spin axis $\underset{\rightarrow}{\mathbf{a}}_i$ of the absolute angular momentum of $\mathcal{W}_i$ about the COM of $\mathcal{W}_i$ is given by [5]

$$h_{ai} = I_{si}\underset{\rightarrow}{\mathbf{a}}_i\cdot\underset{\rightarrow}{\boldsymbol{\omega}} + I_{si}\omega_{si} \ , \ i = 1...n \tag{12}$$

Taking the time derivative of (12) results in

$$\dot{h}_{ai} = I_{si}\dot{\underset{\rightarrow}{\mathbf{a}}}_i\cdot\underset{\rightarrow}{\boldsymbol{\omega}} + I_{si}\underset{\rightarrow}{\mathbf{a}}_i\cdot\dot{\underset{\rightarrow}{\boldsymbol{\omega}}} + I_{si}\dot{\omega}_{si} \ , \ i = 1...n \tag{13}$$

Note that in (13)

$$\begin{aligned}\dot{\underset{\rightarrow}{\mathbf{a}}}_i\cdot\underset{\rightarrow}{\boldsymbol{\omega}} &= (\mathring{\underset{\rightarrow}{\mathbf{a}}}_i + \underset{\rightarrow}{\boldsymbol{\omega}}\times\underset{\rightarrow}{\mathbf{a}}_i)\cdot\underset{\rightarrow}{\boldsymbol{\omega}} = (\underset{\rightarrow}{\boldsymbol{\omega}}\times\underset{\rightarrow}{\mathbf{a}}_i)\cdot\underset{\rightarrow}{\boldsymbol{\omega}} \\ &= \underset{\rightarrow}{\mathbf{a}}_i\cdot(\underset{\rightarrow}{\boldsymbol{\omega}}\times\underset{\rightarrow}{\boldsymbol{\omega}}) = 0\end{aligned} \tag{14}$$

Setting (13) equal to (5) gives

$$I_{si}\underset{\rightarrow}{\mathbf{a}}_i\cdot\dot{\underset{\rightarrow}{\boldsymbol{\omega}}} + I_{si}\dot{\omega}_{si} = g_{ai} \ , \ i = 1...n \tag{15}$$

This equation can be rearranged to solve for $I_{si}\dot{\omega}_{si}$ as follows

$$I_{si}\dot{\omega}_{si} = -I_{si}\underset{\rightarrow}{\mathbf{a}}_i\cdot\dot{\underset{\rightarrow}{\boldsymbol{\omega}}} + g_{ai} \ , \ i = 1...n \tag{16}$$

which relates $\dot{\omega}_{si}$ to $\dot{\underset{\rightarrow}{\boldsymbol{\omega}}}$ as desired. Substituting (16) into (11) allows (11) to be written in terms of $\dot{\underset{\rightarrow}{\boldsymbol{\omega}}}$ to yield

$$\underset{\rightarrow}{\mathbf{J}}\cdot\dot{\underset{\rightarrow}{\boldsymbol{\omega}}} = -\underset{\rightarrow}{\boldsymbol{\omega}}\times\left(\underset{\rightarrow}{\mathbf{J}}\cdot\underset{\rightarrow}{\boldsymbol{\omega}} + \sum_{i=1}^{n}\underset{\rightarrow}{\mathbf{a}}_i I_{si}\omega_{si}\right) + \underset{\rightarrow}{\mathbf{g}} + \sum_{i=1}^{n}\left(I_{si}\underset{\rightarrow}{\mathbf{a}}_i\underset{\rightarrow}{\mathbf{a}}_i\cdot\dot{\underset{\rightarrow}{\boldsymbol{\omega}}} - \underset{\rightarrow}{\mathbf{a}}_i g_{ai}\right) \tag{17}$$

Collecting the $\dot{\underset{\rightarrow}{\boldsymbol{\omega}}}$ terms in this equation results in

$$\left(\underset{\rightarrow}{\mathbf{J}} - \sum_{i=1}^{n}I_{si}\underset{\rightarrow}{\mathbf{a}}_i\underset{\rightarrow}{\mathbf{a}}_i\right)\cdot\dot{\underset{\rightarrow}{\boldsymbol{\omega}}} = -\underset{\rightarrow}{\boldsymbol{\omega}}\times\left(\underset{\rightarrow}{\mathbf{J}}\cdot\underset{\rightarrow}{\boldsymbol{\omega}} + \sum_{i=1}^{n}\underset{\rightarrow}{\mathbf{a}}_i I_{si}\omega_{si}\right) + \underset{\rightarrow}{\mathbf{g}} - \sum_{i=1}^{n}\underset{\rightarrow}{\mathbf{a}}_i g_{ai} \tag{18}$$

Setting

$$\underset{\rightarrow}{\mathbf{J}}^* \triangleq \underset{\rightarrow}{\mathbf{J}} - \sum_{i=1}^{n}I_{si}\underset{\rightarrow}{\mathbf{a}}_i\underset{\rightarrow}{\mathbf{a}}_i \tag{19}$$

then (18) can be written with only one derivative term as

$$\underset{\rightarrow}{\mathbf{J}}^*\cdot\dot{\underset{\rightarrow}{\boldsymbol{\omega}}} = -\underset{\rightarrow}{\boldsymbol{\omega}}\times\left(\underset{\rightarrow}{\mathbf{J}}\cdot\underset{\rightarrow}{\boldsymbol{\omega}} + \sum_{i=1}^{n}\underset{\rightarrow}{\mathbf{a}}_i I_{si}\omega_{si}\right) + \underset{\rightarrow}{\mathbf{g}} - \sum_{i=1}^{n}\underset{\rightarrow}{\mathbf{a}}_i g_{ai} \tag{20}$$

which can be implemented as a nonlinear state-space equation in an EKF with state variable $\underset{\rightarrow}{\boldsymbol{\omega}}$. In this work the EKF was implemented using the $3+n$ nonlinear state-space equations of motion represented by (20) and (5) with corresponding state variables $\underset{\rightarrow}{\boldsymbol{\omega}}$ and $h_{ai}, i = 1...n$.

III. Extended Kalman filter

An EKF is now developed that is based on the formulation presented by Yang [2] but instead of using a reduced quaternion model it includes all four quaternion components and implements the equations of motion derived in the previous section. Yang's formulation assumes the availability of attitude quaternion measurements (from, for example, QUaternion ESTimation (QUEST) [6]) and angular rate measurements (from, for example, a gyroscope). To implement (20) and (5) within the EKF, these vector equations need to be expressed in a frame of reference. Frame $\mathscr{F}_b$ is chosen for convenience since $\underset{\rightarrow}{\boldsymbol{I}}_{\mathcal{W}i}$, $\underset{\rightarrow}{\mathbf{J}}$, $\underset{\rightarrow}{\mathbf{J}}^*$, $\underset{\rightarrow}{\mathbf{b}}_i$, $\underset{\rightarrow}{\mathbf{b}}_{\mathcal{R}}$, and $\underset{\rightarrow}{\mathbf{a}}_i$ are constant when expressed in this reference frame. Using vectrix notation, all vectors and dyadics are expressed in $\mathscr{F}_b$ as follows [5]

$$\begin{aligned}
[\boldsymbol{\omega}\ \dot{\boldsymbol{\omega}}\ \mathbf{a}_i\ \mathbf{g}\ \mathbf{b}_i\ \mathbf{b}_{\mathcal{R}}] &\triangleq \mathscr{F}_b \cdot \left[\underset{\rightarrow}{\boldsymbol{\omega}}\ \underset{\rightarrow}{\dot{\boldsymbol{\omega}}}\ \underset{\rightarrow}{\mathbf{a}}_i\ \underset{\rightarrow}{\mathbf{g}}\ \underset{\rightarrow}{\mathbf{b}}_i\ \underset{\rightarrow}{\mathbf{b}}_{\mathcal{R}}\right] \\
\boldsymbol{I}_{\mathcal{W}i} &\triangleq \mathscr{F}_b \cdot \underset{\rightarrow}{\boldsymbol{I}}_{\mathcal{W}i} \cdot \mathscr{F}_b^{\mathsf{T}} \\
\mathbf{J} &\triangleq \mathscr{F}_b \cdot \underset{\rightarrow}{\mathbf{J}} \cdot \mathscr{F}_b^{\mathsf{T}} \\
\mathbf{J}^* &\triangleq \mathscr{F}_b \cdot \underset{\rightarrow}{\mathbf{J}}^* \cdot \mathscr{F}_b^{\mathsf{T}}
\end{aligned} \tag{21}$$

where $\boldsymbol{\omega}$, $\dot{\boldsymbol{\omega}}$, $\mathbf{a}_i$, $\mathbf{g}$, $\mathbf{b}_i$ and $\mathbf{b}_{\mathcal{R}}$ are 3×1 column matrices containing the components of their respective vectors expressed in $\mathscr{F}_b$. Similarly, $\boldsymbol{I}_{\mathcal{W}i}$, $\mathbf{J}$ and $\mathbf{J}^*$ are the 3×3 inertia matrices corresponding to their moment of inertia dyadics expressed relative to the $\mathscr{F}_b$ axes.

Let $n=3$ reaction wheels for the scope of this paper. Then the resulting equations of motion from (20) and (5) become

$$\begin{aligned}
\dot{h}_{a1} &= g_{a1} + \phi_{01} \\
\dot{h}_{a2} &= g_{a2} + \phi_{02} \\
\dot{h}_{a3} &= g_{a3} + \phi_{03} \\
\dot{\boldsymbol{\omega}} &= \mathbf{J}^{*-1}\left[-\boldsymbol{\omega}^{\times}\left(\mathbf{J}\boldsymbol{\omega} + \sum_{i=1}^{3}\mathbf{a}_i I_{si}\omega_{si}\right) + \mathbf{g} - \sum_{i=1}^{3}\mathbf{a}_i g_{ai}\right] + \boldsymbol{\phi}_1
\end{aligned} \tag{22}$$

where the notation $(\,)^{\times}$ represents the skew-symmetric matrix, ϕ_{0i} and $\boldsymbol{\phi}_1$ correspond to zero-mean process Gaussian noise, and, with $\mathbf{1}$ as the 3×3 identity matrix, (3) and (19) become

$$\begin{aligned}
\mathbf{J} &= \mathbf{J}_b + \sum_{i=1}^{3}\left[\boldsymbol{I}_{\mathcal{W}i} + m_{\mathcal{W}i}\left(b_i^2\mathbf{1} - \mathbf{b}_i\mathbf{b}_i^{\mathsf{T}}\right)\right] \\
\mathbf{J}^* &= \mathbf{J} - \sum_{i=1}^{3} I_{si}\mathbf{a}_i\mathbf{a}_i^{\mathsf{T}}
\end{aligned} \tag{23}$$

The nonlinear quaternion kinematics equations of motion with the addition of process Gaussian noise $\boldsymbol{\phi}_2$ and ϕ_3 are [2]

$$\begin{aligned}
\dot{\mathbf{q}} &= -\frac{1}{2}\boldsymbol{\omega}^{\times}\mathbf{q} + \frac{1}{2}q_0\boldsymbol{\omega} + \boldsymbol{\phi}_2 \\
\dot{q}_0 &= -\frac{1}{2}\boldsymbol{\omega}^{\mathsf{T}}\mathbf{q} + \phi_3
\end{aligned} \tag{24}$$

where $\mathbf{q}$ represents the vector components of the attitude quaternion, q_0 is the scalar component of the attitude quaternion, and the noise has a mean of zero.

The gyroscope drift rate can be modelled by [7]

$$\dot{\boldsymbol{\beta}} = \boldsymbol{\phi}_4 \tag{25}$$

where $\boldsymbol{\beta}$ is the bias drift in the angular velocity measurement and $\boldsymbol{\phi}_4$ corresponds to zero-mean process Gaussian noise.

Referring to the equations of motion (22), let the 13×1 state column matrix $\mathbf{x}=[h_{a1}, h_{a2}, h_{a3}, \boldsymbol{\omega}^{\mathsf{T}}, \mathbf{q}^{\mathsf{T}}, q_0, \boldsymbol{\beta}^{\mathsf{T}}]^{\mathsf{T}}$ and the process noise column matrix $\boldsymbol{\phi}=[\phi_{01}, \phi_{02}, \phi_{03}, \boldsymbol{\phi}_1^{\mathsf{T}}, \boldsymbol{\phi}_2^{\mathsf{T}}, \phi_3, \boldsymbol{\phi}_4^{\mathsf{T}}]^{\mathsf{T}}$ so that the nonlinear state-space equations can be written in the form $\dot{\mathbf{x}} = f(\mathbf{x}, g_{ai}, \mathbf{g}, \boldsymbol{\phi})$. Letting dt be the sampling period and k enumerate the sampling instants, the discrete-time state-space equations used in the EKF prediction phase can be obtained using the finite difference method $\dot{\mathbf{x}} \approx (\mathbf{x}_{k+1} - \mathbf{x}_k)/dt$ as follows

$$\begin{aligned}
\begin{bmatrix} h_{a1k+1} \\ h_{a2k+1} \\ h_{a3k+1} \\ \boldsymbol{\omega}_{k+1} \\ \mathbf{q}_{k+1} \\ q_{0k+1} \\ \boldsymbol{\beta}_{k+1} \end{bmatrix} &= \left(\begin{bmatrix} h_{a1k} \\ h_{a2k} \\ h_{a3k} \\ \boldsymbol{\omega}_k \\ \mathbf{q}_k \\ q_{0k} \\ \boldsymbol{\beta}_k \end{bmatrix} + \begin{bmatrix} g_{a1k} \\ g_{a2k} \\ g_{a3k} \\ \square \\ -\frac{1}{2}\boldsymbol{\omega}_k^{\times}\mathbf{q}_k + \frac{1}{2}q_{0k}\boldsymbol{\omega}_k \\ -\frac{1}{2}\boldsymbol{\omega}_k^{\mathsf{T}}\mathbf{q}_k \\ \mathbf{0} \end{bmatrix} dt \right) + \begin{bmatrix} \phi_{01k} \\ \phi_{02k} \\ \phi_{03k} \\ \boldsymbol{\phi}_{1k} \\ \boldsymbol{\phi}_{2k} \\ \phi_{3k} \\ \boldsymbol{\phi}_{4k} \end{bmatrix} dt \\
\mathbf{x}_{k+1} &= \mathbf{F}(\mathbf{x}_k, g_{aik}, \mathbf{g}_k) + \mathbf{G}(\boldsymbol{\phi}_k)
\end{aligned} \tag{26}$$

where $\square = \mathbf{J}^{*-1}[-\boldsymbol{\omega}_k^{\times}(\mathbf{J}\boldsymbol{\omega}_k + \sum_{i=1}^{3}\mathbf{a}_i I_{si}\omega_{sik}) + \mathbf{g}_k - \sum_{i=1}^{3}\mathbf{a}_i g_{aik}]$, $\mathbf{0}$ is the zero matrix with compatible dimensions, $\mathbf{F}$ is called the state transition matrix, $\mathbf{G}(\boldsymbol{\phi}_k) = \boldsymbol{\phi}_k dt$, ω_{sik} can be calculated from elements of $\mathbf{x}_k$ using (12), and g_{aik} and $\mathbf{g}_k$ are measured torque inputs. Note that $\mathbf{J}^{*-1}$ is constant and, therefore, need only be calculated once prior to beginning the EKF iterations.

The measurements used in the EKF update phase are the reaction wheel speeds ω_{siy}, angular velocity $\boldsymbol{\omega}_y$ (from the gyroscope) and attitude quaternion $\mathbf{q}_y$ and q_{0y} (from, for example, QUEST). The resulting measurement equations including zero-mean Gaussian noise ψ_{0i}, $\boldsymbol{\psi_1}$, $\boldsymbol{\psi_2}$ and ψ_3 are

$$\begin{aligned}
\omega_{s1y} &= \omega_{s1} + \psi_{01} \\
\omega_{s2y} &= \omega_{s2} + \psi_{02} \\
\omega_{s3y} &= \omega_{s3} + \psi_{03} \\
\boldsymbol{\omega}_y &= \boldsymbol{\omega} + \boldsymbol{\beta} + \boldsymbol{\psi}_1 \\
\mathbf{q}_y &= \mathbf{q} + \boldsymbol{\psi}_2 \\
q_{0y} &= q_0 + \psi_3
\end{aligned} \tag{27}$$

Let $\mathbf{y} = [\omega_{s1y}, \omega_{s2y}, \omega_{s3y}, \boldsymbol{\omega}_y^{\mathsf{T}}, \mathbf{q}_y^{\mathsf{T}}, q_{0y}]^{\mathsf{T}}$ be the 10×1 measurement column matrix. The reaction wheel speed ω_{siy_k} can be related to the angular momentum states h_{aik} using (12)

$$\omega_{siy_k} = \frac{h_{aik}}{I_{si}} - \mathbf{a}_i^{\mathsf{T}}\boldsymbol{\omega}_k\ ,\ i = 1...n \tag{28}$$

The resulting observation matrix $\mathbf{H}$ can then be used to relate the measurements to the states as follows

$$\begin{aligned}
\begin{bmatrix} \omega_{s1y_k} \\ \omega_{s2y_k} \\ \omega_{s3y_k} \\ \boldsymbol{\omega}_{y_k} \\ \mathbf{q}_{y_k} \\ q_{0y_k} \end{bmatrix} &= \begin{bmatrix} \frac{1}{I_{s1}} & 0 & 0 & -\mathbf{a}_1^{\mathsf{T}} & \mathbf{0} & 0 & \mathbf{0} \\ 0 & \frac{1}{I_{s2}} & 0 & -\mathbf{a}_2^{\mathsf{T}} & \mathbf{0} & 0 & \mathbf{0} \\ 0 & 0 & \frac{1}{I_{s3}} & -\mathbf{a}_3^{\mathsf{T}} & \mathbf{0} & 0 & \mathbf{0} \\ \mathbf{0} & \mathbf{0} & \mathbf{0} & \mathbf{1} & \mathbf{0} & \mathbf{0} & \mathbf{1} \\ \mathbf{0} & \mathbf{0} & \mathbf{0} & \mathbf{0} & \mathbf{1} & \mathbf{0} & \mathbf{0} \\ 0 & 0 & 0 & \mathbf{0} & \mathbf{0} & 1 & \mathbf{0} \end{bmatrix} \begin{bmatrix} h_{a1k} \\ h_{a2k} \\ h_{a3k} \\ \boldsymbol{\omega}_k \\ \mathbf{q}_k \\ q_{0k} \\ \boldsymbol{\beta}_k \end{bmatrix} + \begin{bmatrix} \psi_{01k} \\ \psi_{02k} \\ \psi_{03k} \\ \boldsymbol{\psi}_{1k} \\ \boldsymbol{\psi}_{2k} \\ \psi_{3k} \end{bmatrix} \\
\mathbf{y} &= \mathbf{H}\mathbf{x} + \boldsymbol{\psi}
\end{aligned} \tag{29}$$

where $\boldsymbol{\psi} = \left[\psi_{01k}, \psi_{02k}, \psi_{03k}, \boldsymbol{\psi}_{1k}^\intercal, \boldsymbol{\psi}_{2k}^\intercal, \psi_{3k}\right]^\intercal$ is the measurement Gaussian noise column matrix, $\mathbf{1}$ is the 3×3 identity matrix and $\mathbf{0}$ is the zero matrix with compatible dimensions.

Taking the partial derivative of the state transition matrix $\mathbf{F}$ from (26) with respect to $\mathbf{x}_k$ gives the state transition Jacobian matrix $\mathbf{F}_{k-1}$ as follows [2]

$$\mathbf{F}_{k-1} \triangleq \frac{\partial \mathbf{F}}{\partial \mathbf{x}_k} \tag{30}$$

This operation takes partial derivatives of the rows of $\mathbf{F}$ with respect to each state variable. For example, referring to (26) let $\mathbf{F}_2$ be the rows of $\mathbf{F}$ corresponding to the vector component of the quaternion. Then $\mathbf{F}_2 = \mathbf{q}_k + (-\frac{1}{2}\boldsymbol{\omega}_k^\times \mathbf{q}_k + \frac{1}{2} q_{0k} \boldsymbol{\omega}_k) dt$. The corresponding partial derivatives of these rows with respect to the state variables are

$$\frac{\partial \mathbf{F}_2}{\partial \mathbf{x}_k} = \begin{bmatrix} \frac{\partial \mathbf{F}_2}{\partial h_{a1k}} & \frac{\partial \mathbf{F}_2}{\partial h_{a2k}} & \frac{\partial \mathbf{F}_2}{\partial h_{a3k}} & \frac{\partial \mathbf{F}_2}{\partial \boldsymbol{w}_k} & \frac{\partial \mathbf{F}_2}{\partial \mathbf{q}_k} & \frac{\partial \mathbf{F}_2}{\partial q_{0k}} & \frac{\partial \mathbf{F}_2}{\partial \boldsymbol{\beta}_k} \end{bmatrix} \tag{31}$$

Evaluating each of the first three of these partial derivatives gives three zero matrices $\mathbf{0}$ of dimension 3×1. The term $\frac{\partial \mathbf{F}_2}{\partial \boldsymbol{w}}$ can be evaluated using the fact that $\frac{\partial (\mathbf{a}^\times \mathbf{b})}{\partial \boldsymbol{w}_k} = \mathbf{a}^\times \frac{\partial \mathbf{b}}{\partial \boldsymbol{w}_k} - \mathbf{b}^\times \frac{\partial \mathbf{a}}{\partial \boldsymbol{w}_k}$

$$\begin{aligned} \frac{\partial \mathbf{F}_2}{\partial \boldsymbol{w}_k} &= \left[-\frac{1}{2} \frac{\partial}{\partial \boldsymbol{w}_k} (\boldsymbol{\omega}_k^\times \mathbf{q}_k) + \frac{1}{2} q_{0k} \mathbf{1} \right] dt \\ &= \left[-\frac{1}{2} (-\mathbf{q}_k^\times) + \frac{1}{2} q_{0k} \mathbf{1} \right] dt \\ &= \frac{1}{2} \left(\mathbf{q}_k^\times + q_{0k} \mathbf{1} \right) dt \end{aligned} \tag{32}$$

where $\mathbf{1}$ is the 3×3 identity matrix. Repeating this partial derivative evaluation for each row of $\mathbf{F}$ yields

$$\mathbf{F}_{k-1} = \begin{bmatrix} 1 & 0 & 0 & \mathbf{0} & \mathbf{0} & 0 & \mathbf{0} \\ 0 & 1 & 0 & \mathbf{0} & \mathbf{0} & 0 & \mathbf{0} \\ 0 & 0 & 1 & \mathbf{0} & \mathbf{0} & 0 & \mathbf{0} \\ \mathbf{0} & \mathbf{0} & \mathbf{0} & \square & \mathbf{0} & \mathbf{0} & \mathbf{0} \\ \mathbf{0} & \mathbf{0} & \mathbf{0} & \frac{1}{2}(\mathbf{q}_k^\times + q_{0k}\mathbf{1})dt & \mathbf{1} - \frac{1}{2}\boldsymbol{w}_k^\times dt & \frac{1}{2}\boldsymbol{w}_k dt & \mathbf{0} \\ 0 & 0 & 0 & -\frac{1}{2}\mathbf{q}_k^\intercal dt & -\frac{1}{2}\boldsymbol{w}_k^\intercal dt & 1 & \mathbf{0} \\ \mathbf{0} & \mathbf{0} & \mathbf{0} & \mathbf{0} & \mathbf{0} & \mathbf{0} & \mathbf{1} \end{bmatrix} \tag{33}$$

where $\square = \mathbf{1} - \mathbf{J}^{*-1}[\boldsymbol{\omega}_k^\times \mathbf{J} - (\mathbf{J}\boldsymbol{\omega}_k + \sum_{i=1}^3 \mathbf{a}_i I_{si} \omega_{sik})^\times] dt$, and $\mathbf{0}$ is the zero matrix of compatible dimensions. Similarly, referring to (26) set $\mathbf{L}_{k-1} \triangleq \frac{\partial \mathbf{G}}{\partial \boldsymbol{\phi}_k} = \mathbf{1} dt$ where the identity matrix $\mathbf{1}$ has dimensions 13×13. Let the process and measurement Gaussian noise have covariance matrices $\mathbf{Q}_k = E(\boldsymbol{\phi}_k \boldsymbol{\phi}_k^\intercal)$ and $\mathbf{R}_k = E(\boldsymbol{\psi}_k \boldsymbol{\psi}_k^\intercal)$, respectively.

A. Prediction phase

Using similar notation as in [2], the EKF iteration begins by first calculating the predicted state $\hat{\mathbf{x}}_{k|k-1}$ using (26)

$$\hat{\mathbf{x}}_{k|k-1} = \mathbf{F}(\hat{\mathbf{x}}_{k-1|k-1}, g_{aik-1}, \mathbf{g}_{k-1}) \tag{34}$$

Note that ω_{sik} in (26) can be calculated from (12) as $\omega_{sik-1|k-1} = \frac{\hat{h}_{aik-1|k-1}}{I_{si}} - \mathbf{a}_i^\intercal \hat{\boldsymbol{\omega}}_{k-1|k-1}, i = 1...n$ where $\hat{h}_{aik-1|k-1}$ and $\hat{\boldsymbol{\omega}}_{k-1|k-1}$ are elements of $\hat{\mathbf{x}}_{k-1|k-1}$.

The notation $\hat{\mathbf{x}}_{k|k-1}$ in (34) can be read as "the state estimate $\hat{\mathbf{x}}$ at the current time step k given the state and measurement information from the previous time step $k-1$". In other words, this current estimate has not yet taken into account the most recent k^{th} measurement (hence the $|k-1$ subscript notation). Similarly, the first $k-1$ subscript of $\hat{\mathbf{x}}_{k-1|k-1}$ in (34) refers to the state estimate $\hat{\mathbf{x}}$ from the previous $k-1$ time step. The second $|k-1$ in the subscript again indicates that the most recent k^{th} measurement information has not yet been accounted for. Also note that the predicted state estimate for the current k^{th} time step $\hat{\mathbf{x}}_{k|k-1}$ uses torque measurements from the previous time step $(g_{aik-1}, \mathbf{g}_{k-1})$.

After the state prediction step is the covariance prediction step. The covariance matrices $\mathbf{P}_{k|k-1}$ and $\mathbf{P}_{k-1|k-1}$ describe the uncertainty of the current state estimate $\hat{\mathbf{x}}_{k|k-1}$ and previous state estimate $\hat{\mathbf{x}}_{k-1|k-1}$, respectively, and are related by

$$\mathbf{P}_{k|k-1} = \mathbf{F}_{k-1} \mathbf{P}_{k-1|k-1} \mathbf{F}_{k-1}^\intercal + \mathbf{L}_{k-1} \mathbf{Q}_k \mathbf{L}_{k-1}^\intercal \tag{35}$$

where the state transition Jacobian $\mathbf{F}_{k-1}$ is evaluated at $(\hat{\mathbf{x}}_{k-1|k-1}, g_{aik-1}, \mathbf{g}_{k-1})$.

B. Update phase

Having completed the prediction phase, the update phase of the EKF calculates the innovation or output prediction error $\tilde{\mathbf{y}}_k$ and innovation covariance $\mathbf{S}_k$ as follows [2]

$$\begin{aligned} \tilde{\mathbf{y}}_k &= \mathbf{y}_k - \mathbf{H}\hat{\mathbf{x}}_{k|k-1} \\ \mathbf{S}_k &= \mathbf{H}\mathbf{P}_{k|k-1}\mathbf{H}^\intercal + \mathbf{R}_k \end{aligned} \tag{36}$$

The Kalman gain $\mathbf{K}_k$ can then be calculated as

$$\mathbf{K}_k = \mathbf{P}_{k|k-1} \mathbf{H}^\intercal \mathbf{S}_k^{-1} \tag{37}$$

The updated state estimate $\hat{\mathbf{x}}_{k|k}$ and updated covariance matrix estimate $\mathbf{P}_{k|k}$ are then calculated using the Kalman gain

$$\begin{aligned} \hat{\mathbf{x}}_{k|k} &= \hat{\mathbf{x}}_{k|k-1} + \mathbf{K}_k \tilde{\mathbf{y}}_k \\ \mathbf{P}_{k|k} &= (\mathbf{1} - \mathbf{K}_k \mathbf{H}) \mathbf{P}_{k|k-1} \end{aligned} \tag{38}$$

The subscript $|k$ in (38) indicates that the most recent k^{th} measurement information has now been accounted for. Note that the updated attitude quaternion in the state estimate needs to be normalized. These updated estimates can then be used in (34) and (35) as $\hat{\mathbf{x}}_{k-1|k-1}$ and $\mathbf{P}_{k-1|k-1}$ to repeat the EKF iteration. Also note that Lefferts *et al.* [3] indicate that since all four quaternion elements are not independent, singularity issues in the covariance matrix result. While these singularities did not occur for the conditions used in this research, there are different approaches that can be applied to overcome this issue [3].

IV. Numerical simulations

The EKF developed in the previous section was validated in simulation on the example 2U CubeSat geometry shown in Fig. 2 consisting of a rigid body $\mathcal{R}$ with three reaction wheel rotors $\mathcal{W}_i$. The asymmetry of the solar panels was exaggerated to highlight the ability of the equations of motion used in the EKF to handle non-diagonal inertia matrices for $\mathcal{R}$. The example CubeSat was designed in SolidWorks 2020 and then exported and simulated in MATLAB R2020b using

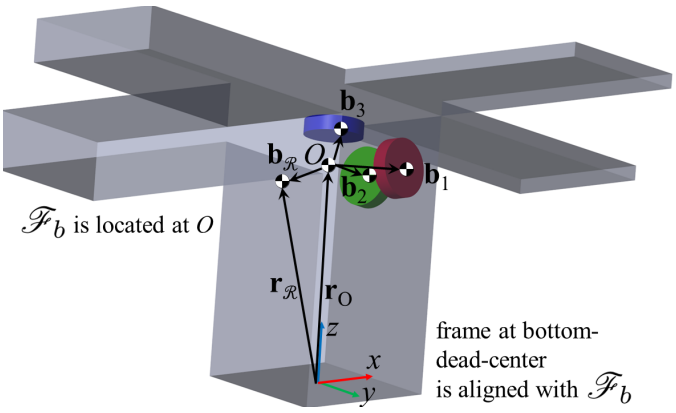

Fig. 2. Example 2U CubeSat geometry $\mathcal{R}$ with reaction wheel rotors $\mathcal{W}_1$, $\mathcal{W}_2$ and $\mathcal{W}_3$ used in simulator to validate EKF

the Simscape Multibody Simulink toolbox. The moments of inertia I_{xx}, I_{yy}, and I_{zz} and products of inertia $I_{xy} = I_{yx}$, $I_{yz} = I_{zy}$, and $I_{xz} = I_{zx}$ of $\mathcal{R}$ (without the reaction wheel rotors $\mathcal{W}_i$) about the COM of $\mathcal{R}$ taken with respect to the $\mathscr{F}_b$ axes were calculated using the Mass Properties window of SolidWorks 2020. Table I summarizes these mass properties.

TABLE I
CUBESAT $\mathcal{R}$ (WITHOUT REACTION WHEEL ROTORS) MASS AND INERTIA

Property	Value
$m_{\mathcal{R}}$	3.8 kg
I_{xx}	0.0359 kgm^2
I_{yy}	0.0398 kgm^2
I_{zz}	0.0483 kgm^2
$I_{yz} = I_{zy}$	-0.0024 kgm^2
$I_{xz} = I_{zx}$	-0.0031 kgm^2
$I_{xy} = I_{yx}$	-0.0014 kgm^2

It is important to recognize that the calculated products of inertia from SolidWorks 2020 shown in Table I are the negative of what are needed in the inertia matrix $\boldsymbol{I}_{\mathcal{R}}$ from (1)

$$\boldsymbol{I}_{\mathcal{R}} = \begin{bmatrix} I_{xx} & -I_{xy} & -I_{xz} \\ -I_{xy} & I_{yy} & -I_{yz} \\ -I_{xz} & -I_{yz} & I_{zz} \end{bmatrix} \tag{39}$$

Note that, as shown in Fig. 2, SolidWorks reported the COM of $\mathcal{R}$ relative to a frame at bottom-dead-center of the CubeSat with axes aligned with $\mathscr{F}_b$. Let the COM of $\mathcal{R}$ from bottom dead center be $\mathbf{r}_{\mathcal{R}}$. Similarly, let the COM of $\mathcal{W}_i$ from bottom-dead-center be $\mathbf{r}_{\mathcal{W}_i}$. Then the location of O (COM of $\mathcal{R}+\mathcal{W}_i$) from bottom dead center can be calculated as

$$\mathbf{r}_O = \frac{1}{m_{\mathcal{R}} + \sum_{i=1}^{3} m_{\mathcal{W}_i}} (m_{\mathcal{R}} \mathbf{r}_{\mathcal{R}} + \sum_{i=1}^{3} m_{\mathcal{W}_i} \mathbf{r}_{\mathcal{W}_i}) \tag{40}$$

from which, referring to Fig. 1, the locations from O to the COM of $\mathcal{R}$ and $\mathcal{W}_i$ can be calculated

$$\begin{aligned} \mathbf{b}_{\mathcal{R}} &= \mathbf{r}_{\mathcal{R}} - \mathbf{r}_O \\ \mathbf{b}_1 &= \mathbf{r}_{\mathcal{W}_1} - \mathbf{r}_O \\ \mathbf{b}_2 &= \mathbf{r}_{\mathcal{W}_2} - \mathbf{r}_O \\ \mathbf{b}_3 &= \mathbf{r}_{\mathcal{W}_3} - \mathbf{r}_O \end{aligned} \tag{41}$$

Noting that all vectors and dyadics in this section are expressed relative to axes aligned with $\mathscr{F}_b$, Table II summarizes the results of these calculations for the simulated example CubeSat. The orientation of the rotor spin axes can

TABLE II
COM AND ROTOR MASS AND INERTIA PROPERTIES FOR CUBESAT

Property	Value
$m_{\mathcal{W}_i}, i = 1..3$	0.0126 kg
I_{si}	2.51×10^{-6} kgm^2
I_{ti}	1.36×10^{-6} kgm^2
$\mathbf{r}_{\mathcal{R}}$	$[-0.0237, -0.0158, 0.1403]^\mathsf{T}$ m
$\mathbf{r}_{\mathcal{W}_1}$	$[0.0375, 0.0250, 0.1500]^\mathsf{T}$ m
$\mathbf{r}_{\mathcal{W}_2}$	$[0.0000, 0.0375, 0.1500]^\mathsf{T}$ m
$\mathbf{r}_{\mathcal{W}_3}$	$[0.0000, 0.0000, 0.1750]^\mathsf{T}$ m
$\mathbf{r}_O$	$[-0.0233, -0.0154, 0.1404]^\mathsf{T}$ m
$\mathbf{b}_{\mathcal{R}}$	$[-0.00036, -0.00036, -0.00018]^\mathsf{T}$ m
$\mathbf{b}_1$	$[0.0608, 0.0404, 0.0096]^\mathsf{T}$ m
$\mathbf{b}_2$	$[0.0233, 0.0529, 0.0096]^\mathsf{T}$ m
$\mathbf{b}_3$	$[0.0233, 0.0154, 0.0346]^\mathsf{T}$ m

be arbitrarily set, but for the scope of this simulation they have been defined as $\mathbf{a}_1 = [1\ 0\ 0]^\mathsf{T}$, $\mathbf{a}_2 = [0\ 1\ 0]^\mathsf{T}$ and $\mathbf{a}_3 = [0\ 0\ 1]^\mathsf{T}$.

Band-limited Gaussian process noise $\boldsymbol{\phi}$ was added to the simulated EKF model with variances σ^2 for each noise signal of $\sigma^2_{\phi_{0_i}} = 1\times10^{-9}$ (kgm^2/s^2)^2, $\sigma^2_{\boldsymbol{\phi}_1} = 1\times10^{-8}$ (rad/s^2)^2, $\sigma^2_{\boldsymbol{\phi}_2} = \sigma^2_{\phi_3} = 1\times10^{-5}$ s^{-2}, and $\sigma^2_{\boldsymbol{\phi}_4} = 1\times10^{-5}$(rad/s^2)^2. Similarly band-limited Gaussian measurement noise $\boldsymbol{\psi}$ was added with variances $\sigma^2_{\psi_{0_i}} = 1$(rad/s)^2, $\sigma^2_{\boldsymbol{\psi}_1} = 1\times10^{-5}$(rad/s)^2, and $\sigma^2_{\boldsymbol{\psi}_2} = \sigma^2_{\psi_3} = 1\times10^{-2}$. Diagonal matrices with these process and measurement noise variances were used to form $\mathbf{Q}_k$ and $\mathbf{R}_k$, respectively. Since, in practice, the actual inertia cannot be precisely known, 5% model uncertainty was added to the calculated inertia $\mathbf{J}$ used in the EKF. Sinusoidal external disturbance torques $\mathbf{g}$ of frequency 0.1Hz having amplitude 2×10^{-5}Nm about the body x-axis and 5×10^{-5}Nm about the body y- and z-axes were applied. Similarly, sinusoidal reaction wheel motor torques g_{a_i} of frequency 0.1Hz having amplitude 1.5×10^{-4}Nm were applied. It was assumed that $\mathbf{g}$ and g_{a_i} used in the EKF model were measured with a Gaussian noise variance of $\sigma^2_{\mathbf{g}} = 1\times10^{-10}$(Nm)^2 and $\sigma^2_{g_{a_i}} = 1\times10^{-9}$(Nm)^2, respectively. The EKF initial conditions for the state vector were randomly set.

The equations of motion derived in Section II were implemented and, when no noise was added, the results matched those from the Simscape Multibody toolbox as desired — effectively validating the derived equations of motion and their implementation. Process and measurement noise were then added to the simulator and the EKF was simulated for 500s using a sample rate of 1Hz. Fig. 3 plots the resulting CubeSat body angular velocity components as a function of time. In each subplot, the actual angular velocity is shown as a dashed-red line, the noisy and biased gyroscope measurements are superimposed as dotted blue lines, and the EKF estimated angular rates are plotted as a solid black line. It can be seen in this figure that, despite the presence of noise and gyroscope drift, the EKF is able to converge towards the actual angular rates as desired.

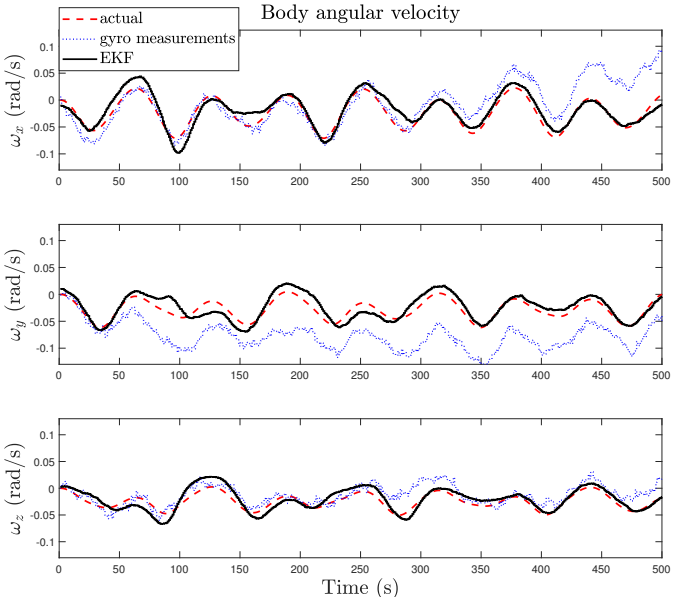

Fig. 3. Simulation results for body angular velocity $\boldsymbol{\omega}$

Similarly, Fig. 4 plots the corresponding four attitude quaternion components as a function of time consisting of the vector components (q_x, q_y, q_z) and scalar component q_0. Similar to Fig. 3, the actual quaternion components are plotted as a red-dashed line, the noisy quaternion measurements are plotted as a blue dotted line, and the EKF estimated quaternion components are plotted as a solid black line. It can be seen that, despite the randomly-incorrect initial conditions, the EKF is able to converge towards the actual quaternion components.

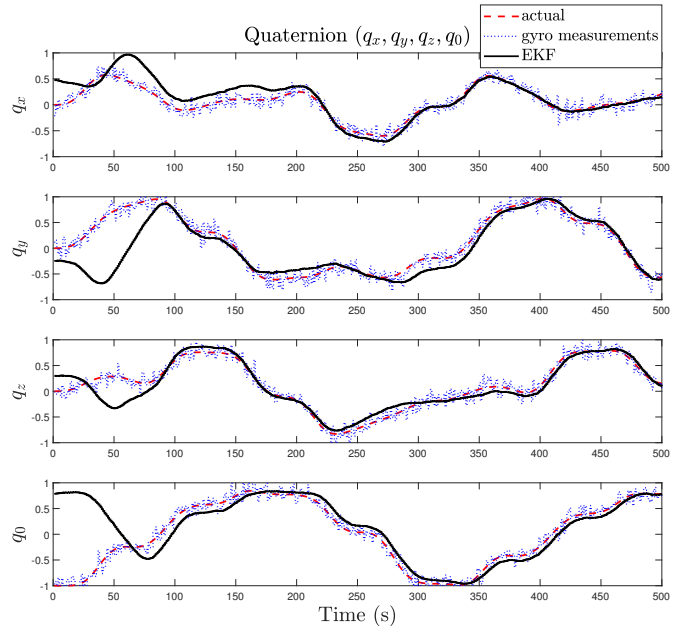

Fig. 4. Simulation results for attitude quaternion vector components $\mathbf{q} = (q_x, q_y, q_z)$ and scalar component q_0

Lastly, Fig. 5 plots the gyroscope bias drift as a function of time. The actual bias is shown as a red-dashed line while the EKF bias estimate is shown as a black solid line. Note that this bias is measured as part of the gyroscope angular velocity measurement — bias itself is not directly measured. It can be seen from this figure that the EKF bias estimates are able to converge towards the actual bias as desired.

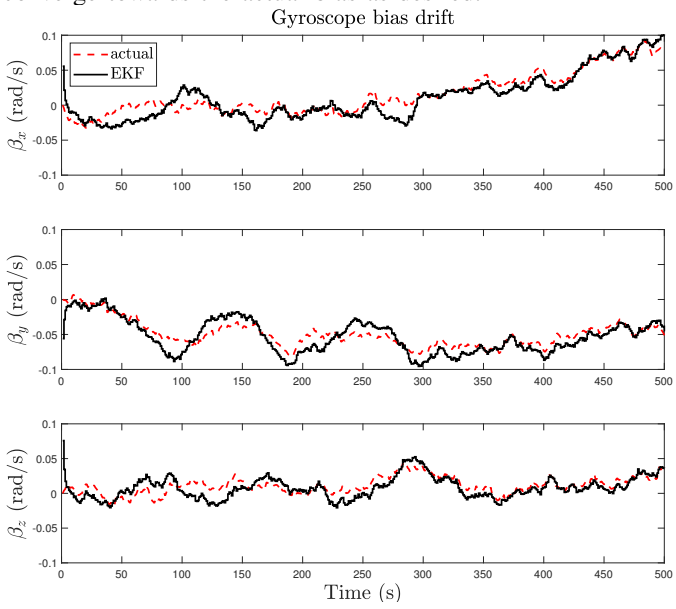

Fig. 5. Simulation results for gyroscope bias drift $\boldsymbol{\beta}$

V. Conclusions

This paper derives the equations of motion for a general rigid body with n arbitrarily-positioned and arbitrarily-oriented reaction wheels. It then demonstrates how these nonlinear attitude dynamics equations can be used in an extended Kalman filter formulation by creating a nonlinear state-space equation using states that include the angular momentum of the reaction wheels as well as the angular velocity of the rigid body. Additional states in the EKF include the attitude quaternion and gyroscope bias. Numerical simulations are then carried out using an example CubeSat geometry to validate the derived equations of motion and corresponding EKF formulation. For the simulation conditions used in this research, the results demonstrate that the EKF is able to converge towards the actual CubeSat's attitude quaternion and body angular velocity as desired.

References

[1] A. Erlank, W. Steyn, "Arcminute attitude estimation for CubeSats with a novel nano star tracker," IFAC Proceedings Volumes, vol. 47, no. 3, pp. 9679–9684, 2014.

[2] Y. Yaguang, "Spacecraft modeling, attitude determination, and control quaternion-based approach," CRC Press, 2019.

[3] E. Lefferts, F. Markley, M Shuster, "Kalman filtering for spacecraft attitude estimation," Journal of Guidance, Control and Dynamics, vol. 5, no. 5, pp. 417–429, 1982.

[4] Y. Yang, Z. Zhou, "Spacecraft dynamics should be considered in Kalman filter based attitude estimation," 26th AAS/AIAA Space Flight Mechanics Meeting, Napa, CA, 2016.

[5] P. Hughes, "Spacecraft attitude dynamics", John Wiley & Sons, Inc., 1986.

[6] M. Shuster, S. Oh, "Three-axis attitude determination from vector observations," Journal of Guidance and Control, vol. 4, no. 1, pp. 70-77, 1981.

[7] R. Farrenkopf, "Analytic steady-state accuracy solutions for two common spacecraft attitude estimators," Journal of Guidance and Control, vol. 1, no. 4, pp. 282-284, 1978.